Bull Math Biol (2011) 73:2430–2451
DOI 10.1007/s11538-011-9631-y

ORIGINAL ARTICLE

# A Continuum Mathematical Model of the Developing Murine Retinal Vasculature

**M. Aubert · M.A.J. Chaplain · S.R. McDougall · A. Devlin · C.A. Mitchell**

Received: 30 April 2010 / Accepted: 11 January 2011 / Published online: 1 February 2011


**Abstract** Angiogenesis, the process of new vessel growth from pre-existing vasculature, is crucial in many biological situations such as wound healing and embryogenesis. Angiogenesis is also a key regulator of pathogenesis in many clinically important disease processes, for instance, solid tumour progression and ocular diseases. Over the past 10–20 years, tumour-induced angiogenesis has received a lot of attention in the mathematical modelling community and there have also been some attempts to model angiogenesis during wound healing. However, there has been little modelling work of vascular growth during normal development. In this paper, we describe an in silico representation of the developing retinal vasculature in the mouse, using continuum mathematical models consisting of systems of partial differential equations. The equations describe the migratory response of cells to growth factor gradients, the evolution of the capillary blood vessel density, and of the growth factor concentration. Our approach is closely coupled to an associated experimental programme to parameterise our model effectively and the simulations provide an excellent correlation with in vivo experimental data. Future work and development of this model will enable us to elucidate the impact of molecular cues upon vasculature development and the implications for eye diseases such as diabetic retinopathy and neonatal retinopathy of prematurity.

**Keywords** Angiogenesis · Retina · Chemotaxis · Growth factors · Astrocytes

M. Aubert (✉) · M.A.J. Chaplain
Division of Mathematics, University of Dundee, Dundee DD1 4HN, Scotland, UK
e-mail: marine@maths.dundee.ac.uk

M. Aubert · S.R. McDougall
Institute of Petroleum Engineering, Heriot-Watt University, Edinburgh EH14 4AS, Scotland, UK

A. Devlin · C.A. Mitchell
Biomedical Sciences Research Institute, University of Ulster, Coleraine BT52 1SA, Northern Ireland

## 1 Introduction

Angiogenesis is the dominant process of new blood vessel formation by which endothelial cells sprout from an existing vasculature and form new (flowing) vessels. This is a crucial process in embryogenesis, organ growth, and wound healing, generating a functional vascular network which matches the metabolic requirements of the tissue. Angiogenesis is also a fundamental step in pathological situations such as tumour development, arthritis, and ocular diseases including retinopathy of prematurity, age-related macular degeneration, and diabetic retinopathy (Folkman 1995).

Tumour-induced angiogenesis has received a lot of attention in the mathematical modelling community going back to the paper of Balding and McElwain (1985). The modelling has focused on the role played by endothelial cells during the formation of blood vessels. The models have typically considered the proliferation and the migration of endothelial cells in response to signalling cues. In particular, these models have introduced soluble and diffusible angiogenic factors (such as VEGF) produced by the cells of the tumour bulk and insoluble extracellular matrix macromolecules (e.g. fibronectin). The interactions of the endothelial cells with angiogenic factors and the macromolecules of the extracellular matrix can be described in a set of nonlinear partial differential equations (PDEs). In these continuum models, the endothelial cells migrate in response to signalling cues from a parent vessel, across and through the extracellular matrix until they reach the solid tumour (Anderson and Chaplain 1998; Orme and Chaplain 1997). In some models, a discrete element has been introduced in order to describe the migration of individual endothelial cells and the formation of individual blood vessels (Anderson and Chaplain 1998; Levine et al. 2001). To complete the study, blood flow remodelling in a tumour-induced vascular network has been also considered (Alarcon et al. 2003; Chaplain et al. 2006; Macklin et al. 2009; McDougall et al. 2002, 2006; Stéphanou et al. 2005, 2006). More recently, Owen et al. (2009) studied vascular remodelling during growth of normal and cancerous tissues.

Angiogenesis during wound healing has been the subject of modelling investigations. Most models describe the formation of blood vessel after a wound by using a system of PDEs. Xue et al. (2009) developed an 8 variable model incorporating densities of macrophages, fibroblasts, endothelial tip cells and capillary sprouts, concentrations of angiogenic factors (PDGF and VEGF), and density of extracellular matrix. Schugart et al. (2008) adopt a similar approach. Other models considered further simplified systems. Olsen et al. (1997) proposed a 2 variable model in order to investigate the roles of the extracellular matrix on the proliferative and migratory response of endothelial cells. Gaffney et al. (2002) presented an other example of a 2 constituent model which describes the passive motion of capillary sprouts following their leading tip cell. Some models additionally incorporated the chemotactic response of endothelial cells to angiogenic factors (Byrne and Chaplain 1995; Byrne et al. 2000; Chaplain 1995; Pettet et al. 1996a, 1996b) or oxygen (Flegg et al. 2009). Finally, recent work has examined the role of angiogenesis and its impact on the oxygenation of tissue in tissue engineering, with implications for reconstructive microsurgery (Matzavinos et al. 2009).

The angiogenic process involved during the formation of the retinal vasculature network has been less well studied by the modelling community. However,

elucidating how a complex retinal vascular plexus is formed is of utmost importance, since an abnormal vascular network formation is involved in eye diseases, such as retinopathy of prematurity and diabetic retinopathy (Folkman 1995). The formation of the retinal vascular plexus (RVP), similar to other developing organ systems, is mediated by Vascular Endothelial Growth Factor-A (herein termed VEGF) which induces endothelial cell migration and division. Around birth in mice, endothelial cells begin to migrate from the optic nerve chiasm over the surface of the inner retina (Gerhardt et al. 2003; Fruttiger et al. 1996). VEGF is a major chemotactic factor for endothelial cells in the retina, with VEGF inhibition preventing endothelial cell migration and formation of the retinal plexus (Gerhardt et al. 2003; Uemura et al. 2006). The formation of the endothelial cell network is dependent on astrocytes which migrate from the region of the optic nerve in advance of endothelial cells (Stone et al. 1995). Astrocytes guide the formation of the retinal vascular plexus as they produce VEGF in the unvascularised retina and provide a template over which endothelial cells migrate (Dorrell et al. 2002; West et al. 2005). Astrocyte migration is further dependent on the presence of a gradient of PDGF-A, produced by underlying retinal ganglion cells. The rate of astrocyte migration in transgenic mice that constitutively express high levels of PDGF-A in retinal ganglion cells is delayed, probably reflecting a loss of concentration gradient driven chemotaxis. Additionally, retinal ganglion cell-specific PDGF over-expressing mice have a significantly denser astrocyte network, indicating that astrocyte number is correlated to PDGF-A concentration (Fruttiger et al. 1996; West et al. 2005). Murine astrocytic network formation begins shortly before birth and growth of the superficial RVP begins on the day of birth (post-natal day 0), eventually covering the inner surface of the retina by post-natal day 8. In this study, we correlate the rate of astrocyte and endothelial cell migration determined from in vivo experiments in mice to the simulation results.

Our aim is to focus on physiological angiogenesis in the retina during the development of the embryonic and neonatal mouse eye. We have developed a combined mathematical and biological approach. This aims to investigate the roles of molecular cues on the developing plexus. The data generated from our in vivo experiments are used to inform the mathematical modelling approach for model parameterisation and validation purposes. We first focus on the formation of the superficial plexus. We developed two mathematical models for the retinal vascular network. The first, basic model is restricted to three equations describing the migration of endothelial tip cells and the migratory response of the blood vessels, following the path created by the tips. We also consider the evolution of VEGF concentration and its effect on tip migration. In the second model, we improved our basic model in order to consider the migratory response of astrocytes to a gradient of PDGF and the secretion of VEGF by hypoxic astrocytes. The computational simulation results of our model are compared with experimental data.

## 2 In vivo Experimental Results

We quantified the extend of astrocyte and endothelial cell migration at various developmental stages during retinal vascular plexus (RVP) formation: from embryonic

day (E)15.5 to post-natal day (P)8. The time of birth (P0) corresponds approximately to E21.

C57BL/J6 mice were euthanised at various pre- and post-natal stages. Following immediate enucleation and fixation of the globe, retinal whole mounts were prepared as previously described in Gerhardt et al. (2003). In order to flat mount the spherical retina on glass slides, 3–4 incisions toward the optic nerve were made. All animal procedures were approved by and conformed to UK Home Office Guidelines. The retina were stained with the astrocytic nuceli marker rabbit anti-Pax2 antibody (Covance, Leeds, UK) in order to detect astrocyte nuclei and with isolectin-B4 biotin-conjugate (*Griffonia simplicifolia* [GSI-B4]: Sigma, Gillingham, UK) in order to detect endothelial cells. Anti-rabbit Alexa-Fluor 488 and Streptavidin-conjugated Alexa-Fluor 633 antibodies (Invitrogen, Paisley, UK) were used as appropriate fluorophores. Images were captured using a SP5 confocal microscope (Lecia Microsystems GmbH, Wetzlar, Germany).

Migration of astrocytes and endothelial cells were observed at E15.5, E18.5, P0, P3, P5, and P8 (Figs. 1 and 2). Mean of the distance from the optic nerve to the radial extent of astrocyte and endothelial cell migration was quantified using at least 4 samples at each developmental stage (Fig. 2). We also quantified the standard errors of the mean (SEM). SEM is estimated by the sample standard deviation divided by the square root of the sample size ($n = 4$–$6$ at each time point).

## 3 Mathematical Model

Our model describes the migration of endothelial cells in response to VEGF. We restrict our attention to one spatial dimension, in the direction of the line connecting the centre of the optic nerve to the edge of the retina. We started from the model initially developed by Gaffney et al. (2002) to describe the migration of the capillary tips and the migratory response of blood vessels, dragged along the flux of the tips. We added the evolution of VEGF concentration and its effect on tip migration as performed in Schugart et al. (2008), Xue et al. (2009). We denote the averaged capillary tip density by $n(x,t)$, the blood capillary density by $b(x,t)$ and the VEGF concentration by $c(x,t)$ at position $x$ and time $t$.

### 3.1 The Capillary Tip Density Equation

The conservation equation for the capillary tip density $n$ is given by

$$\frac{\partial n}{\partial t} = -\nabla.J_n + f(n,b), \tag{1}$$

where $J_n$ is the capillary tip flux and $f(n,b)$ describes the tip kinetics.

We take the tip flux $J_n$ to be:

$$J_n = -D_1\nabla n - D_2 n\nabla b + \chi_0 n\nabla c. \tag{2}$$

The flux term reflects the assumption that the capillary tips migrate via a biased random walk. The first term influencing the motion of capillary tips is random motility.

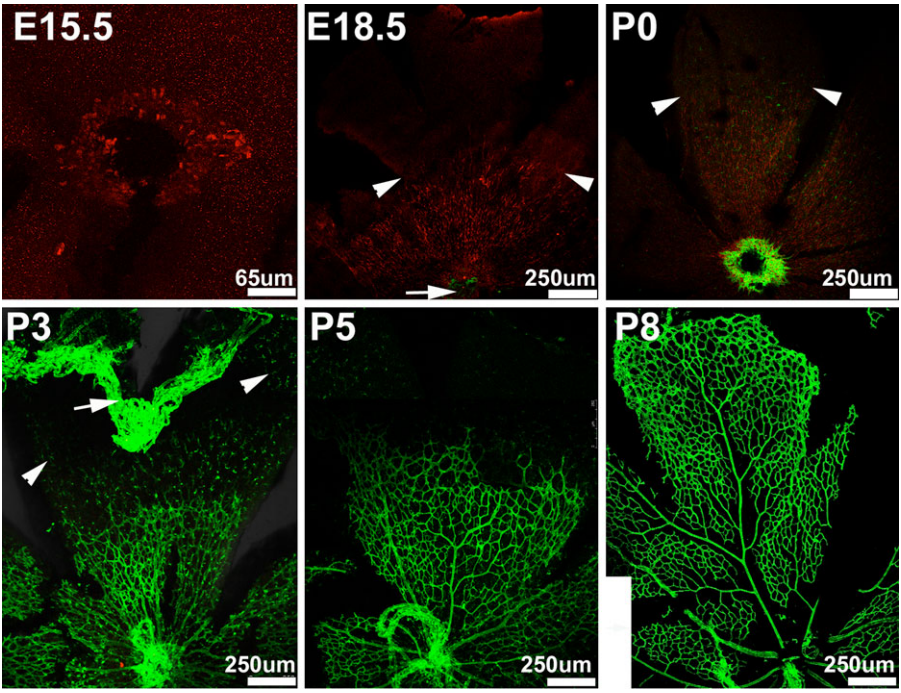


**Fig. 1** Murine retinal astrocyte migration and retinal vascular plexus formation. Typical confocal images of Pax2 (astrocytes, *red*) and isolectin B4 (endothelial cells, *green*) immunostained retinal wholemounts at various pre- and post-natal stages. 400× image showing Pax2 astrocytes are only located in the optic nerve head at E15.5. 100× images illustrate astrocyte migration from the optic nerve head (*arrow*) at E18.5 and P0 (*arrowheads* indicated Pax2 extent). Endothelial cell sprouting from the optic nerve begins at P0, and a vascular plexus reaches the retinal edge by P8. At P3, isolectin B4 positive microglial cells (*arrow heads*) and remnants of the embryonic hyaloid vasculature (*arrow*) can also be observed. At P3, the plexus is dense and highly branched but by P5 defined arterioles and venules have formed, and significant remodelling form a sparse network by P8

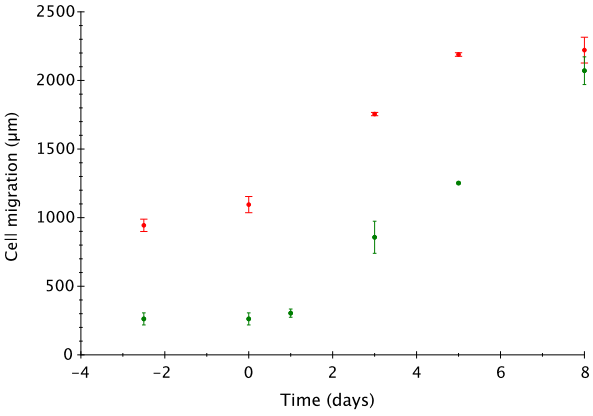


**Fig. 2** Plot showing the in vivo experimental measurement of migration of astrocytes (*in red*) and capillary tips (*in green*) during formation of the superficial retinal vascular plexus as a function of time. Distances were measured from the centre of the optic nerve

The bias is modelled by the two other terms. The first term $-D_2 n\nabla b$ models the migration of capillary tips in the direction of decreasing blood capillary density (Gaffney et al. 2002). It has been introduced to avoid migration of tips in regions which already constrains blood vessels as it is never the case experimentally (data not shown). The second bias term $\chi_0 n\nabla c$ represents the chemotactic response which leads to motion in the direction of increasing VEGF concentration (Anderson and Chaplain 1998; Pettet et al. 1996a).

We modelled the tip kinetics by the three contributions:

$$f(n,b) = \lambda_2 n - \lambda_3 n^2 - \lambda_4 nb. \tag{3}$$

The first term describes the generation of new tips (tip branching) at a rate $\lambda_2$. The second term represents the formation of loops created by two capillary tips (tip-tip anastomosis) at a rate $\lambda_3$, while the last term describes the joining of a tip to a side of a capillary (tip-capillary anastomosis) at a rate $\lambda_4$ (Gaffney et al. 2002; Schugart et al. 2008; Xue et al. 2009).

### 3.2 The Blood Capillary Density Equation

We assume that the blood vessels passively follow their leading tip as modelled in Gaffney et al. (2002), Schugart et al. (2008), Xue et al. (2009). The blood vessels are dragged along the flux of the capillary tips, moving in the same direction with a velocity $v_b$ proportional to the capillary tip velocity: $v_b = h(n)v_n$. The proportional coefficient $h(n)$ depends on the density of capillary tips as the blood vessel velocity $v_b$ should be small when the capillary tip density $n$ is small. So $h(n)$ is assumed to be proportional to the capillary tip density $n$ (Schugart et al. 2008). More precisely $h(n)$ is a non-dimensional parameter equal to the density of endothelial tip cells divided by the initial density of blood vessels: $h(n) = \lambda_5 n/b_0$ and $v_b = h(n)J_n/n = \lambda_5 J_n/b_0$. Therefore, the relation between the flux of the blood capillary density $J_b$ and the flux of the capillary tips is given by

$$J_b = bv_b = -\lambda_5 \frac{b}{b_0}(D_1\nabla n + D_2 n\nabla b - \chi_0 n\nabla c) \tag{4}$$

where $\lambda_5$ is the (average) number of endothelial cells in a capillary tip (Gaffney et al. 2002).

The kinetics of blood capillaries are modelled by the three contributions used by Gaffney et al. (2002):

$$g(n,b) = \nu_0 b(b_0 - b) + \mu_0 nb(b_1 - b) + \lambda_5(\lambda_3 n^2 + \lambda_4 nb). \tag{5}$$

The first term describes the proliferation of endothelial cells according to an ordinary logistic growth at a rate $\nu_0$ and a carrying capacity of $b_0$. The second term represents another contribution to the proliferation, at a rate proportional to the tip density $n$ with a carrying capacity of $b_1$. The third term describes the contribution from tip-tip and tip-capillary anastomoses to blood capillary density.

### 3.3 The VEGF Concentration Equation

The VEGF concentration equation is given by

$$\frac{\partial c}{\partial t} = \underbrace{\lambda_1 S(b)}_{\text{production}} + \underbrace{D_3 \nabla^2 c}_{\text{diffusion}} - \underbrace{\gamma n c}_{\text{consumption}} - \underbrace{\omega c}_{\text{degradation}}, \tag{6}$$

where

$$S(b) = \begin{cases} 1 - b/\hat{b}, & b \le \hat{b}, \\ 0, & b > \hat{b}. \end{cases} \tag{7}$$

The first term describes the production of VEGF according to the function $S(b)$ similar to the one used by Maggelasis and Savakis (1996). VEGF production is controlled by the density of blood vessel carrying oxygen. We assume that if there are no blood vessels, the tissue is therefore hypoxic and will produce VEGF to attract capillary tips. We also assume that when the density of blood capillaries is above a critical level $\hat{b}$, the oxygen concentration delivered by these capillaries will be high enough to supply the oxygen demands of the tissue. Thus, VEGF production will be stopped. Conversely, if the density of blood vessels falls below $\hat{b}$, an increase in VEGF production occurs. The second term represents the diffusion of VEGF into the surrounding tissue with a coefficient $D_3$. The binding of VEGF to tip receptors is modelled in the third term. The last term describes the natural decay at a rate $\omega$.

### 3.4 The Non-dimensionalised System

The dimensional system is therefore composed of the three equations:

$$\frac{\partial n}{\partial t} = \underbrace{D_1 \nabla^2 n}_{\text{diffusion}} + \underbrace{D_2 \nabla (n \nabla b)}_{\text{movement away from capillaries}} - \underbrace{\chi_0 \nabla (n \nabla c)}_{\text{chemotaxis}} + \underbrace{f(n,b)}_{\text{kinetics}}, \tag{8}$$

$$\frac{\partial b}{\partial t} = \underbrace{\frac{\lambda_5}{b_0}\left[D_1 \nabla (b \nabla n) + D_2 \nabla (bn \nabla b) - \chi_0 \nabla (bn \nabla c)\right]}_{\text{capillaries follow tips}} + \underbrace{g(n,b)}_{\text{kinetics}}, \tag{9}$$

$$\frac{\partial c}{\partial t} = \underbrace{\lambda_1 S(b)}_{\text{production}} + \underbrace{D_3 \nabla^2 c}_{\text{diffusion}} - \underbrace{\gamma n c}_{\text{consumption}} - \underbrace{\omega c}_{\text{degradation}}, \tag{10}$$

where

$$f(n,b) = \lambda_2 n - \lambda_3 n^2 - \lambda_4 nb, \tag{11}$$

$$g(n,b) = \nu_0 b(b_0 - b) + \mu_0 nb(b_1 - b) + \lambda_5\left(\lambda_3 n^2 + \lambda_4 nb\right), \tag{12}$$

$$S(b) = \begin{cases} 1 - b/\hat{b}, & b \le \hat{b}, \\ 0, & b > \hat{b}. \end{cases} \tag{13}$$

We non-dimensionalise the system using the following scalings for the variables:

$$\tilde{n} = \frac{n}{n_0}, \qquad \tilde{b} = \frac{b}{b_0}, \qquad \tilde{c} = \frac{c}{c_0}, \qquad \tilde{t} = \frac{t}{T}, \qquad \tilde{x} = \frac{x}{x_0}.$$

By omitting the tildes for clarity, we obtain the non-dimensional system:

$$\frac{\partial n}{\partial t} = \underbrace{C_1\nabla^2 n}_{\text{diffusion}} + \underbrace{C_2\nabla(n\nabla b)}_{\text{movement away from capillaries}} - \underbrace{\chi\nabla(n\nabla c)}_{\text{chemotaxis}} + \underbrace{f(n,b)}_{\text{kinetics}}, \tag{14}$$

$$\frac{\partial b}{\partial t} = \underbrace{k_5\left[C_1\nabla(b\nabla n) + C_2\nabla(bn\nabla b) - \chi\nabla(bn\nabla c)\right]}_{\text{capillaries follow tips}} + \underbrace{g(n,b)}_{\text{kinetics}}, \tag{15}$$

$$\frac{\partial c}{\partial t} = \underbrace{k_1 S(b)}_{\text{production}} + \underbrace{C_3\nabla^2 c}_{\text{diffusion}} - \underbrace{\eta n c}_{\text{consumption}} - \underbrace{\sigma c}_{\text{degradation}}, \tag{16}$$

where

$$f(n,b) = k_2 n - k_3 n^2 - k_4 n b, \tag{17}$$

$$g(n,b) = \nu b(1-b) + \mu n b\left(1 - \frac{b}{\beta_1}\right) + k_5\left(k_3 n^2 + k_4 n b\right), \tag{18}$$

$$S(b) = \begin{cases} 1 - b/\beta_2, & b \le \beta_2, \\ 0, & b > \beta_2, \end{cases} \tag{19}$$

where the non-dimensionalised parameters are:

$$C_1 = \frac{D_1 T}{x_0^2}, \qquad C_2 = \frac{D_2 T b_0}{x_0^2}, \qquad C_3 = \frac{D_3 T}{x_0^2}, \qquad \chi = \frac{\chi_0 T c_0}{x_0^2},$$

$$\beta_1 = \frac{b_1}{b_0}, \qquad \beta_2 = \frac{\hat{b}}{b_0}, \qquad k_1 = \frac{\lambda_1 T}{c_0}, \qquad k_2 = \lambda_2 T,$$

$$k_3 = \lambda_3 T n_0, \qquad k_4 = \lambda_4 T b_0, \qquad k_5 = \frac{\lambda_5 n_0}{b_0},$$

$$\eta = \gamma T n_0, \qquad \sigma = \omega T, \qquad \nu = \nu_0 T b_0, \qquad \mu = \mu_0 T n_0 b_1.$$

### 3.5 Parameter Values

The average radius from the centre of the optic nerve to the edge of the murine retina is around 2200 μm (2221 ± 94 μm). We thus take the length scale $x_0$ to be 2200 μm. We assume that the domain goes from $x = 0$ to $x = 1$ with $x = 0$ defined as the centre of the optic nerve and $x = 1$ the edge of the retina. The time scale $T$ is taken to be 1 day = 86 400 seconds to match the experimental time scale.

Some of the parameter values can be estimated from the literature.

In Anderson and Chaplain (1998), the authors use the value $10^{-10}$ cm$^2$ s$^{-1}$ for the diffusion coefficient of capillary tips. This parameter value give the non-dimensional value $C_1 = 1.8 \times 10^{-4}$. In Gaffney et al. (2002), the authors choose to take $C_1 = C_2$.

In order to parameterise the value of the chemotactic coefficient Anderson and Chaplain (1998) used the work of Stokes et al. (1990). The authors quantified the chemotactic response of human micro-vessel endothelial cells to acidic fibroblast growth factor (aFBF; now termed FGF1). The chemotactic coefficient $\chi_0$ was found to be $2600 \pm 750$ cm$^2$ s$^{-1}$ M$^{-1}$ (for an aFGF concentration of $10^{-10}$ M). This would lead, in our model, to the non-dimensional value $0.33 < \chi < 0.60$.

As $\lambda_2$ is defined to be the tip branching rate, we can assume $k_2$ to be estimated from the doubling time of tip cells. This is estimated in Gaffney et al. (2002) via the typical doubling time of a proliferating cell (20–24 hours). They thus take $k_2 = (24/20) \ln 2 \approx 0.83$. The same value is used for $k_3$.

Estimates for the diffusion coefficient of VEGF are in range $2.9 \times 10^{-7}$ cm$^2$ s$^{-1}$–$5.9 \times 10^{-6}$ cm$^2$ s$^{-1}$ (Anderson and Chaplain 1998; Bray 1992; Sherratt and Murray 1992). This yields the non-dimensional value $0.5 < C_3 < 10.5$.

For the following parameters, $k_4$, $k_5$ and $\beta_1$, we used the values proposed by Gaffney et al. (2002). Those values are estimated from biological data (Dyson et al. 1992) ($\beta_1 = 9.29$) or to satisfy mathematical conditions ($k_4 = 0.85$ and $k_5 = 0.25$).

Some other parameters are difficult to estimate. Thus, in some cases, we made an assumption regarding some parameter values ($\eta$, $\sigma$ and $\beta_2$) and we chose some others in order to fit the experimental data ($k_1$, $\nu$ and $\mu$).

Likewise, the binding rate of VEGF to capillary tip receptors $\gamma$ and the natural decay $\omega$ are not known. However, the values of the corresponding non-dimensional parameters have been estimated from the literature: $\eta = 0.1$ (Anderson and Chaplain 1998) in the case of a tumour-induced angiogenesis and $\sigma = 0.5$ (Maggelasis and Savakis 1996) in the first attempt of capillary growth modelling in the retina. Thus, we used the given parameter values.

The ratio $\beta_2$ of the critical density of new blood vessels $\hat{b}$ (density above which the concentration of oxygen is high enough to supply the oxygen demands of the tissue) compared to the normal density of blood vessel $b_0$ has been chosen arbitrarily ($\beta_2 = 0.3$).

The production rate of VEGF $\lambda_1$, which must be large enough to stimulate endothelial migration and growth from the blood vessels and thus supply the oxygen demands of the tissue, is extremely difficult to measure experimentally, especially in in vivo conditions. Therefore, the corresponding non-dimensional parameter $k_1$ will be carefully estimated following a sensitivity analysis.

The non-dimensional blood vessel proliferation rates $\nu$ and $\mu$ has been chosen to maintain a maximum value of the non-dimensional capillary density around 1.0.

### 3.6 Initial and Boundary Conditions

The initial conditions are defined for $t = 0$, corresponding to time of birth (P0).

At $t = 0$ the tip cells are located at the edge of the optic nerve (Fig. 1), around 260 µm from the geometric centre of the retina ($262 \pm 44$ µm). In our non-dimensional system, it corresponds to $x = \alpha = 0.12$. The capillary tip density has the form:

$$n(x, t = 0) = n_{\text{init}} e^{-(x-\alpha)^2/\epsilon_1}, \tag{20}$$

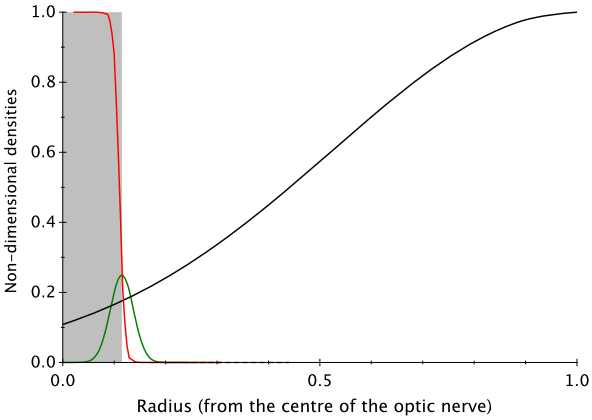


**Fig. 3** Plot showing the initial profiles of capillary tip density (*in green*), blood capillary density (*in red*), and VEGF concentration (*in black*) as a function of the distance from the centre of the optic nerve. The *grey area* delimits the optic nerve region

where $\epsilon_1 = 10^{-3}$ and $n_{\text{init}} = 0.25$.

The blood capillaries are located behind the tip cells and the initial capillary density has the form:

$$b(x, t = 0) = \begin{cases} 1, & x \leq \alpha, \\ 0, & x > \alpha. \end{cases} \tag{21}$$

We assume the presence of a VEGF gradient at time $t = 0$. The concentration of VEGF is supposed to be equal to 1 at the right boundary corresponding to the edge of the retina and decreases to reach its minimum value at the centre of the optic nerve (left boundary). The profile of VEGF concentration is described by the initial condition:

$$c(x, t = 0) = e^{-(1-x)^2/\epsilon_2}, \tag{22}$$

where $\epsilon_2 = 0.45$.

The initial profiles are given in Fig. 3.

We assume that the density of blood vessel in the optic nerve should remain constant. Whereas at the centre of the optic nerve, the density of capillary tips and the concentration of VEGF (except at $t = 0$) should be negligible. Hence, the boundary conditions at the centre of the optic nerve ($x = 0$) are

$$n(0, t) = 0, \qquad b(0, t) = 1, \qquad c(0, t) = 0 \quad \text{for } t > 0,$$
$$\frac{\partial n}{\partial x}(0, t) = \frac{\partial b}{\partial x}(0, t) = \frac{\partial n}{\partial x}(0, t) = 0,$$

At $x = 1$, the following no-flux boundary conditions are used:

$$\frac{\partial x}{\partial t}(1, t) = \frac{\partial b}{\partial x}(1, t) = \frac{\partial n}{\partial x}(1, t) = 0,$$

## 4 Computational Simulation Results

The simulations are performed in COMSOL Multiphysics (©1998–2010 COMSOL AB) using the finite element method to solve the PDE system. The parameter values used in the simulations (unless specified otherwise) are: $C_1 = C_2 = 1.8 \times 10^{-4}$, $C_3 = 10^{-2}$, $\chi = 0.133$, $k_1 = 0.1$, $k_2 = k_3 = 0.83$, $k_4 = 0.85$, $k_5 = 0.25$, $\eta = 0.1$, $\sigma = 0.5$, $\nu = 1$, $\mu = 5$, $\beta_1 = 9.29$, $\beta_2 = 0.3$.

### 4.1 Generic Profiles

The computational simulation profiles of the capillary tip density are shown in Fig. 4 for different time steps corresponding to P0, P1, P3, P5, and P8. It should be noted that the capillary tips start to migrate at P0 from the edge of the optic nerve located at $\alpha = 0.12$, as discussed in Sect. 3.6 and shown in Fig. 1. By P8 the capillary tips have migrated almost completely across the domain (Figs. 1 and 2). It is also important to note that there is very little spreading of capillary tips. The bulk of cell density retains a shape similar to the initial distribution. This is because the motion is largely governed by chemotaxis with the small amount of random movement.

The solution of the complete system is shown in Fig. 5 at P8. A peak of capillary tips (in green), closely followed by the blood vessels (in red), can be observed moving through the domain representing the retina.

### 4.2 Chemotaxis Parameter

In order to examine the importance of chemotaxis in the model, we consider the system for different values of the chemotactic coefficient $\chi$ (Fig. 6). The maximal density of capillary tips is dependent on $\chi$. By P3, the maximal density of capillary tips reaches a position located around $0.395x_0 \approx 870$ μm when $\chi = 0.1$ whereas the maximal density of capillary tips are more than half way through the domain ($0.87 \approx 1920$ μm) when $\chi = 0.4$. As tip cells are approximately 860 μm ($857 \pm 117$ μm) across the retina in vivo by P3, Fig. 6 indicates that the correct value for $\chi$ is close to 0.1. One can notice that a small change in the value of the chemotactic parameter

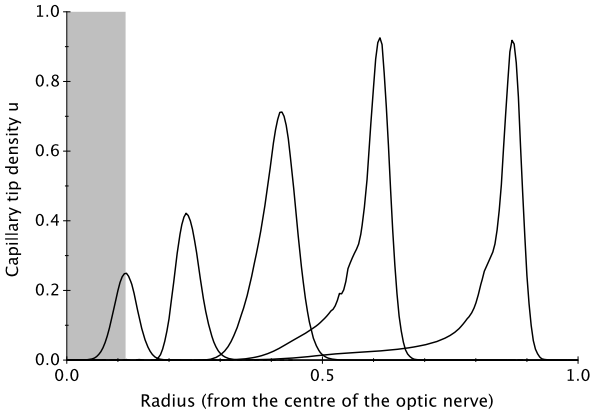


**Fig. 4** Plot showing the capillary tip density as a function of the distance from the centre of the optic nerve at P0, P1, P3, P5, and P8. The *grey area* delimits the optic nerve region

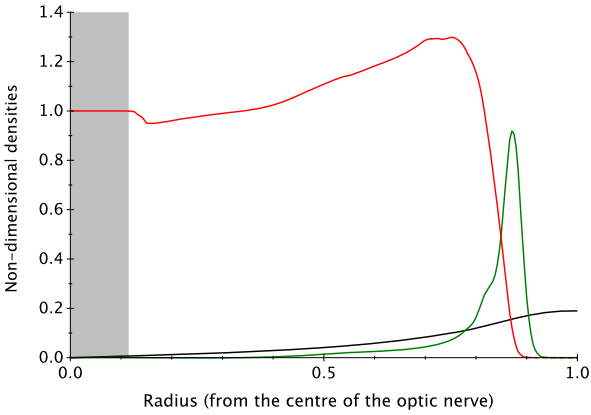


**Fig. 5** Plot showing the capillary tip density (*in green*), blood capillary density (*in red*) and VEGF concentration (*in black*) as a function of the distance from the centre of the optic nerve at P8. The *grey area* delimits the optic nerve region

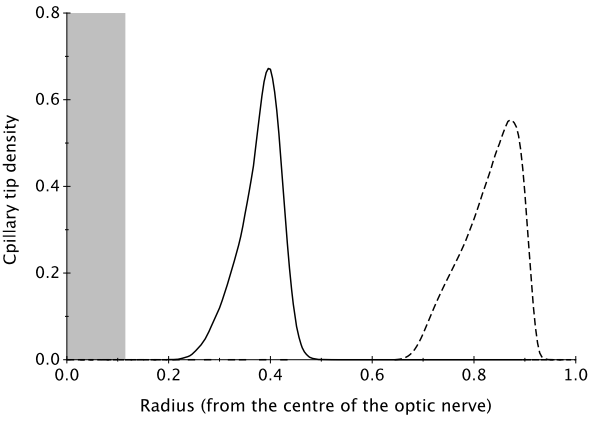


**Fig. 6** Plot showing the capillary tip density as a function of the distance from the centre of the optic nerve at P3 for $\chi = 0.1$ (*solid line*) and $\chi = 0.4$ (*dashed line*). The *grey area* delimits the optic nerve region

significantly affects the rate of migration, indicating chemotaxis is the major factor governing capillary tip motion.

In Fig. 7, we further investigate the relationship between capillary tip speed and chemotactic coefficient by determining the time needed for the maximal density of capillaries to reach the position $x_t = 0.8x_0$ ($\approx 1800$ μm) for a range of chemotactic parameter values. Experimentally, this observation takes place between P5 and P8 (Fig. 2) and more precisely between P7 and P8 (data not shown). The speed of the tip cells depends strongly on the chemotactic coefficient which increases nonlinearly with the chemotactic coefficient. The analysis presented allows us to produce an estimate for the value of the chemotactic coefficient: $0.115 < \chi < 0.135$. We thus find that $\chi_0$ should range from 650 to 760 $\text{cm}^2\,\text{s}^{-1}\,\text{M}^{-1}$.

This analysis reveals that the value of the chemotactic coefficient has been overestimated in Sect. 3.5. This is not surprising given that the experiments presented in Stokes et al. (1990) were performed in vitro with a different kind of cells and an other growth factor than the VEGF which is the focus of this investigation. Furthermore, our model is simplified and would need an extension in order to realistically reproduce the migration of endothelial cells in the retina (cf. Sect. 6).

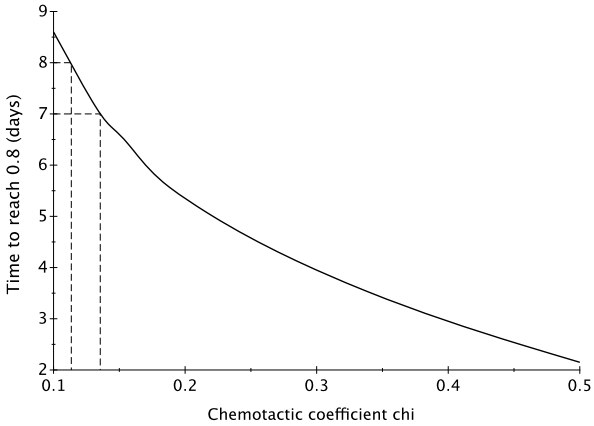


**Fig. 7** Plot showing the time to reach $x = 0.8x_0$ as a function of the non-dimensional chemotactic coefficient ($\chi$)

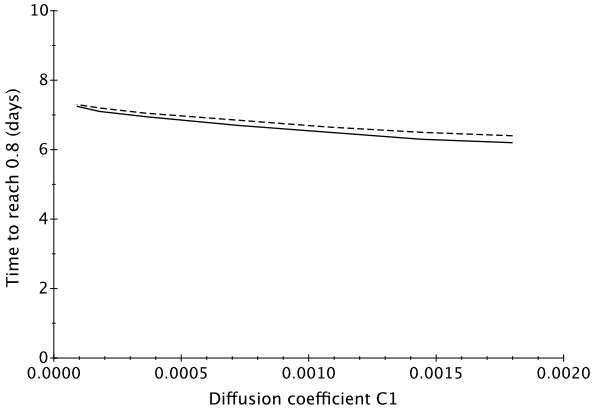


**Fig. 8** Plot showing the time to reach $x = 0.8x_0$ as a function of the non-dimensional diffusion coefficient of the capillary tip cells ($C_1$), if $C_2 = C_1$ (*solid line*) and if $C_2 = 0$ (*dashed line*)

## 5 Parameter Sensitivity Analysis

As discussed in the last subsection (Sect. 4.2) the migration of the capillary tips is largely governed by chemotaxis. We now perform a parameter sensitivity analysis on a set of selected parameters which can play a subordinate role in capillary tip migration by altering the values of the selected parameters and determining the time when the maximal density of capillary tips reaches the position $x_t = 0.8x_0$ ($\approx 1800$ μm). In vivo endothelial tip cells reach this position between P7 and P8.

From Fig. 8, we see that if the tip cells reach $x_t$ between P7 and P8, the non-dimensional diffusion coefficient of the tip cells $C_1$ must be smaller than $4.0 \times 10^{-4}$. To prevent significant spreading of the profile for the tip cells we thus keep $D_1 < 2.2 \times 10^{-10}$ cm$^2$ s$^{-1}$.

Figure 9 reveals that rate of tip cells migration is correlated to the value of the VEGF diffusion coefficient and a value of $0.010 < C_3 < 0.025$ fits the experimental data. This value is 25 to 50 times smaller than the one expected in Sect. 3.5. The coefficient diffusion of VEGF $D_3$ may vary between $5.6 \times 10^{-9}$ and $1.4 \times 10^{-8}$ cm$^2$ s$^{-1}$.

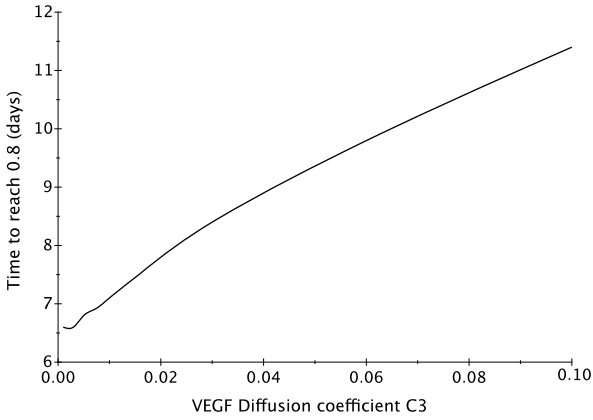


**Fig. 9** Plot showing the time to reach $x = 0.8x_0$ as a function of the non-dimensional diffusion coefficient of VEGF ($C_3$)

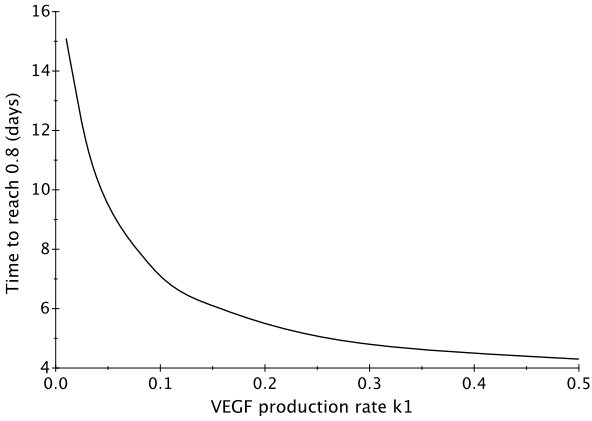


**Fig. 10** Plot showing the time to reach $x = 0.8x_0$ as a function of the non-dimensional production rate of VEGF ($k_1$)

From Fig. 10, we obtain the non-dimensional production rate of VEGF $k_1$ which should range from 0.08 to 0.10 in order to fit the in vivo observations. Therefore, $\lambda_1$ may vary between $0.08c_0$ M/day and $0.1c_0$ M/day.

The simulation results presented in Fig. 11 indicate that the branching parameter value should be between 0.5 and 0.9. The branching and anastomosis rates therefore range from $5.8 \times 10^{-6}$ to $10^{-5}$ $s^{-1}$.

## 6 Model Extension

In this extension to the original model, we also consider another cell type, astrocytes, and the growth factor which guides astrocyte migration, PDGF-A. In the embryonic mouse eye, astrocytes emerge from the optic nerve region and start to migrate across the inner surface of the retina in response to a chemotactic growth factor gradient of PDGF-A (Fruttiger et al. 1996) between E15.5 and E18.5 (Fig. 1). It is important to note that the migration of astrocytes begins before birth although the migration of capillary tips and blood capillaries only begins shortly after birth (Fig. 1). We denote the astrocyte non-dimensional density by $a$ and the PDGF concentration by $p$.

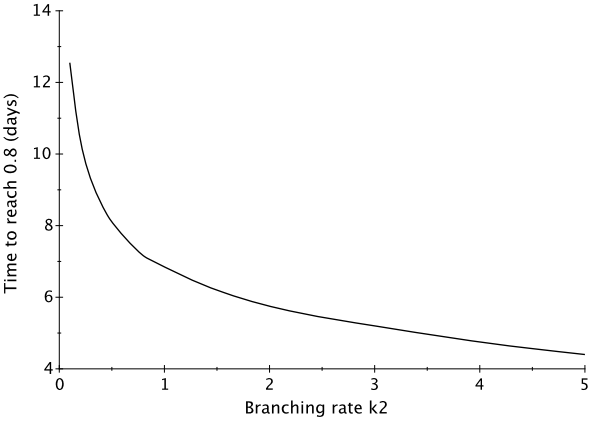


**Fig. 11** Plot showing the time to reach $x = 0.8x_0$ as a function of the branching and tip-tip anastomosis rates ($k_2 = k_3$)

## 6.1 System of Partial Differential Equations

The non-dimensional system is as follows:

$$\frac{\partial n}{\partial t} = \underbrace{C_1\nabla^2 n}_{\text{diffusion}} + \underbrace{C_2\nabla(n\nabla b)}_{\text{movement away from capillaries}} - \underbrace{\chi\nabla(n\nabla c)}_{\text{chemotaxis}} + \underbrace{f(n,b)}_{\text{kinetics}}, \tag{23}$$

$$\frac{\partial b}{\partial t} = \underbrace{k_5\big[C_1\nabla(b\nabla n) + C_2\nabla(bn\nabla b) - \chi\nabla(bn\nabla c)\big]}_{\text{capillaries follow tips}} + \underbrace{g(n,b)}_{\text{kinetics}}, \tag{24}$$

$$\frac{\partial c}{\partial t} = \underbrace{k_1 a S(b)}_{\text{production}} + \underbrace{C_3\nabla^2 c}_{\text{diffusion}} - \underbrace{\eta n c}_{\text{consumption}} - \underbrace{\sigma c}_{\text{degradation}}, \tag{25}$$

$$\frac{\partial a}{\partial t} = \underbrace{C_4\nabla^2 a}_{\text{diffusion}} - \underbrace{\psi\nabla(a\nabla p)}_{\text{chemotaxis}} + \underbrace{\nu_a a(1-a)}_{\text{kinetics}}, \tag{26}$$

$$\frac{\partial p}{\partial t} = \underbrace{C_5\nabla^2 p}_{\text{diffusion}} - \underbrace{\eta a p}_{\text{kinetics}}, \tag{27}$$

where

$$f(n,b) = k_2 n - k_3 n^2 - k_4 nb, \tag{28}$$

$$g(n,b) = \nu b(1-b) + \mu nb\left(1 - \frac{b}{\beta_1}\right) + k_6\big(k_3 n^2 + k_4 nb\big), \tag{29}$$

$$S(b) = \begin{cases} 1 - b/\beta_2, & b \le \beta_2, \\ 0, & b > \beta_2. \end{cases} \tag{30}$$

The dimensionless parameters previously defined remain the same except for:

$$k_1 = \frac{\lambda_1 T a_0}{c_0}.$$

Equations (23) and (24) are equivalent to the previous ones (14) and (15). In this PDE system, the VEGF equation (25) is similar to the previous model equation (16), except for the production term as VEGF production is now controlled by the astrocyte density $a$.

As for the capillary tips, we model astrocyte migration via a biased random walk. The random motility is described in the first term with a non-dimensional diffusion coefficient $C_4$. The bias is modelled by the second term, the chemotaxis migration with a chemotactic coefficient $\psi$ (motion in the direction of increasing PDGF concentration). The kinetic term reflects the proliferation of astrocytes according to an ordinary logistic growth at a rate $\nu_a$.

In this model, the PDGF-A is initially present in the retina (cf. Sect. 6.3), to reflect the production of PDGF-A by ganglion cells and their precursors. PDGF-A diffuses at a coefficient $C_5$ and binds to astrocyte receptors at a rate $\nu_a$.

### 6.2 Parameter Values

Most of the parameter values from the three-species model remain the same: $C_1 = C_2 = 1.8 \times 10^{-4}$, $C_3 = 10^{-2}$, $k_1 = 0.1$, $k_2 = k_3 = 0.83$, $k_4 = 0.85$, $k_5 = 0.25$, $\eta = 0.1$, $\sigma = 0.5$, $\nu = 1$, $\mu = 5$, $\beta_1 = 9.29$, $\beta_2 = 0.3$.

Only the value of chemotactic coefficient to VEGF, $\chi$, differs from its given value. In our extended model, the non-dimensionalised chemotactic coefficient $\chi$ is greater than the one used in the 3 PDE model (0.5 compared to 0.133). This is due to the different initial conditions of VEGF. In fact, in the first model, the capillary tip migration starts with a pre-existing gradient of VEGF (Fig. 3) whereas in the extended model, VEGF is only produced by the astrocytes as they migrate over the retina, presenting a different VEGF profile (Fig. 13).

The newly added parameters, $\nu_a$ and $\psi$, have been chosen in order to fit the experimental data. The non-dimensional production rate of astrocytes $\nu_a$ has been chosen to maintain a density in the order of 1.0 when astrocytes are presents. Thus, we chose $\nu_a = 0.5$.

The value used for the PDGF chemotactic coefficient $\psi$ used to guide astrocyte migration seems to be small ($\psi = 0.08$). One could expect $\psi$ to be almost equal to $\chi$ in the three-species model, i.e. $\psi = 0.133$. This is explained by the fact that evolution of PDGF is slightly different to the evolution of VEGF in the three-species model: for simplicity, we do not consider PDGF degradation. Considering PDGF degradation would lead to a decrease in PDGF concentration and in order to keep a similar rate of astrocyte migration we would have to increase PDGF chemotactic coefficient.

### 6.3 Initial Conditions

We run our simulations from E17 (i.e. four days prior to the birth $t_0 = -4$) to P8 ($t = 8$). The astrocyte density, the VEGF and PDGF concentrations start to evolve at

$t = t_0$ even though the capillary tips and the blood capillaries migrate from $t = t_C = 0.5$ (corresponding to P0.5).

For $t = [t_0, t_C]$, the capillary tip and blood capillary densities have the form:

$$n(x,t) = n_{\text{init}} e^{-(x-\alpha)^2/\epsilon_1}, \tag{31}$$

$$b(x,t) = \begin{cases} 1, & x \leq \alpha, \\ 0, & x > \alpha, \end{cases} \tag{32}$$

where $\epsilon_1 = 10^{-3}$, $n_{\text{init}} = 0.25$ and $\alpha = 0.12$ (as defined in Sect. 3.6).

In this model, VEGF is only produced by astrocytes and is initially set to 0:

$$c(x,t_0) = 0. \tag{33}$$

The astrocytes are initially located in the optic nerve region and the astrocyte density profile has the form:

$$a(x,t_0) = \begin{cases} 1, & x \leq \alpha, \\ 0, & x > \alpha. \end{cases} \tag{34}$$

We assume the presence of a gradient of PDGF at time $t = t_0$. The concentration of PDGF is supposed to be equal to 1 at the right boundary corresponding to the edge of the retina and decreases to reach its minimum value at the centre of the optic nerve (left boundary). The profile of PDGF concentration is described by the initial condition:

$$p(x,t_0) = e^{-(1-x)^2/\epsilon_2}, \tag{35}$$

where $\epsilon_2 = 0.45$.

### 6.4 Computational Simulations

The parameter values used in the simulations are: $C_1 = C_2 = C_4 = 1.8 \times 10^{-4}$, $C_3 = C_5 = 10^{-2}$, $\chi = 0.5$, $\psi = 0.08$, $k_1 = 0.1$, $k_2 = k_3 = 0.83$, $k_4 = 0.85$, $k_5 = 0.25$, $\eta = 0.1$, $\sigma = 0.5$, $\nu = 1$, $\mu = 5$, $\nu_a = 0.5$, $\beta_1 = 9.29$, $\beta_2 = 0.3$.

The computational simulation profiles of the astrocyte density are shown in Fig. 12 for different time steps corresponding to E17, E18.5, P0, P1, P3, P5, and P8. The astrocytes start to migrate at E17 ($t = t_0$) from the edge of the optic nerve located at $\alpha = 0.12$. Figure 12 shows that astrocytes have almost reached the edge of the domain by P5. It is also important to note that there is very little spreading of capillary tips.

The density and concentration profiles are shown in Fig. 13 at time $t_C$ when the tip cells and the blood vessels are assumed to start their migration. The main difference for capillary tip and blood capillary evolution in this extended model is due to the altered VEGF profile (dashed black line). This profile differs from the previous one (cf. Fig. 3) as VEGF is now produced by astrocytes.

The solution of the astrocyte, tip cell and blood vessel densities are shown in Fig. 14 at P5. Astrocytes (in black) migrate ahead of a peak of capillary tips (in green), closely followed by the blood vessels (in red), moving through the domain representing the retina.

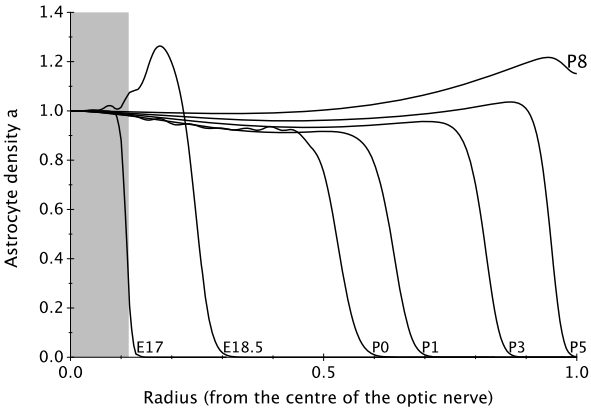


**Fig. 12** Plot showing the astrocyte density as a function of the distance from the centre of the optic nerve at time E17, E18.5, P0, P1, P3, P5, and P8. The *grey area* delimits the optic nerve region

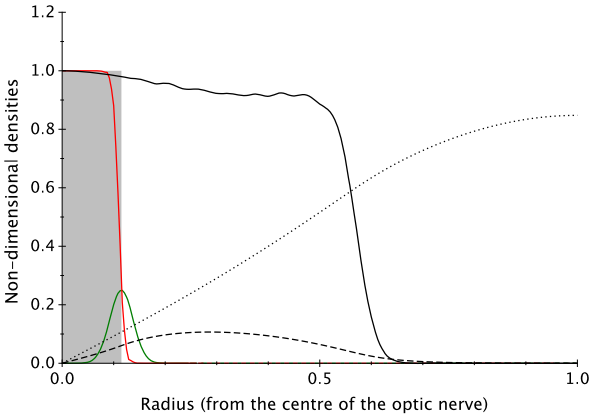


**Fig. 13** Plot showing the capillary tip density (*in green*), blood capillary density (*in red*), astrocyte density (*in black*), VEGF concentration (*dashed black line*), and PDGF concentration (*dotted black line*) as a function of the distance from the centre of the optic nerve at $t_C$ (P05). The *grey area* delimits the optic nerve region

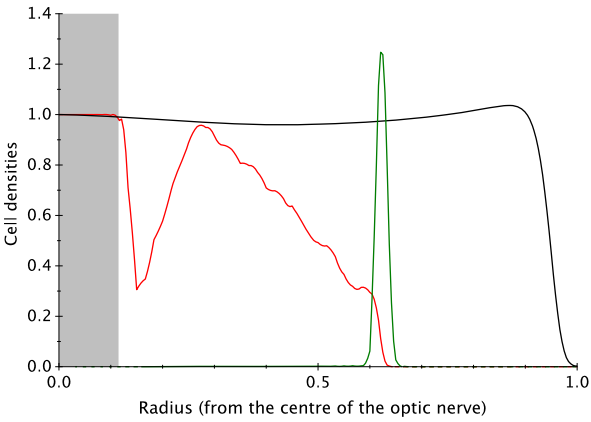


**Fig. 14** Plot showing the capillary tip density (*in green*), blood capillary density (*in red*) and astrocyte density (*in black*) as a function of the distance from the centre of the optic nerve at P5. The *grey area* delimits the optic nerve region

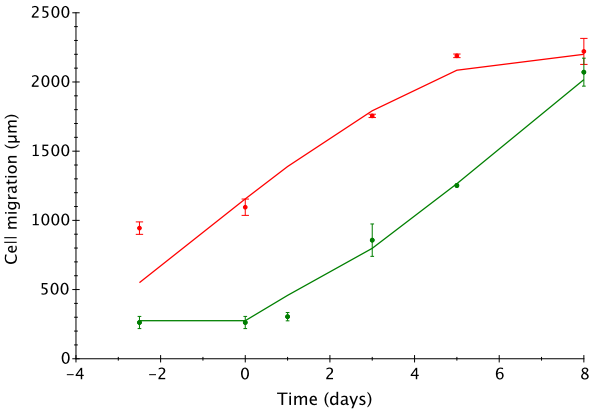


**Fig. 15** Plot showing a comparison of experimental data (*circles with error bars*) with the simulations data (*full lines*) for capillary tip (*in red*) and astrocyte (*in green*) migration during formation of the superficial retinal vascular plexus as a function of time. Distances were measured from the centre of the optic nerve

### 6.5 Comparison with Experimental Data

In Fig. 15, we show a comparison of the experimental data with the results obtained from our simulations. The figure illustrates the migration of astrocytes and endothelial cells as a function of time (from E18.5 to P8). In the computational simulations, the astrocyte migration corresponds to the position where the astrocyte density is equal to 0.5 and the capillary tip migration is estimated where the tip density is set to its maximum. The errors bars in experimental data are the SEM. In the simulations, the errors made by estimating the position of the cells is less than 10 µm (not shown in the figure for clarity).

The simulation results match nicely the experimental data when astrocytes start to migrate at E17 and the tip cells at P0.5.

## 7 Discussion

In this paper, we have presented a model using partial differential equations to reproduce the developing retinal vasculature in one spatial dimension. We compared the computational simulation results of our five variable model incorporating capillary tip density, blood vessel density, astrocyte density, VEGF concentration, and PDGF concentration with experimental data. We showed that our model reproduces the extent and rate of endothelial tip cell and astrocyte migration in the murine eye. One can note the presence of kinks and oscillations in the density of astrocytes, blood vessels, and capillary tips. This reflect a persistence in history due to our initial conditions. We do not consider these features as important fact as they do not change the positions reached by the fastest endothelial cells and astrocytes, which are the only results that we can compare to biological data at that time.

Our approach is a first step in order to investigate and model the key parameters influencing the development of the retinal vasculature. We started our study with a three-species model allowing us to change the parameter values and to perform a complete sensitivity analysis. This model gives good results but the agreement with the experimental data, albeit promising, is far from perfect. One of the major reasons

is the simplification in VEGF production. This study has shown that the migration of cells is largely governed by chemotaxis. Therefore, if the VEGF profile does not exactly reflect the biological phenomenon happening in the developing retina, the migration of the capillary tips will not be realistic enough. Without introducing the astrocytes, it is difficult to set a profile for the concentration of VEGF and to model its evolution as VEGF is produced by the developing astrocytic network. To be more realistic, the initial VEGF profile in the three-species model should be similar to the one obtain in the five-species model (considering the astrocyte migration). Unfortunately, such a profile is impossible to determine without modelling the astrocyte migration and proliferation. Therefore, we must take into account these cells and their dynamic (stimulated by PDGF). Indeed, as can be seen from Fig. 15 the computational simulation results from the full five-variable model provide an excellent correlation with in vivo experimental data.

As chemotaxis plays a important role, it is crucial to determine the value of each chemotactic coefficient. Once the non-dimenionalised chemotactic coefficient is determined, estimated values of dimensional chemotactic coefficient $\chi_0$ can be established. The latter is inversely proportional to the non-dimensionalisation parameter $c_0$. For example, in the three PDE system, we considered $c_0$ as the initial concentration of VEGF on the edge of the retina (right boundary). Unfortunately, it is impossible to experimentally determine the concentration of VEGF in vivo, making it impossible to give an accurate value for $c_0$ and in turn parameters depending on this value such as $\chi_0$ and $\lambda_1$ (and similarly for $\psi_0$ which depends on PDGF concentration $p_0$). Nevertheless, this modelling approach provides a way in which such parameters can be estimated.

We are aware that our model cannot generate the complete vascular structure but nevertheless this system of PDEs allow us to highlight the most important parameters responsible for the migration of the endothelial cells and the astrocytes.

We are currently expanding this work by creating a 2-dimensional hybrid model of retinal vascular plexus development. This discrete model will provide further information on the role of the different cell types and chemotactic signalling factors in the post-natal murine eye. Additionally this model will incorporate flow-mediated remodelling events in order to recapitulated the vascular pruning observed during the migration of the retinal vascular plexus.

**Acknowledgement** The authors gratefully acknowledge the support of the BBSRC grant: BB/F002254/1.

## References

Alarcon, T., Byrne, H., & Maini, P. K. (2003). A cellular automaton model for tumour growth in inhomogeneous environment. *Journal of Theoretical Biology*, *225*(2), 257–274.

Anderson, A. R. A., & Chaplain, M. A. J. (1998). Continuous and discrete mathematical models of tumour-induced angiogenesis. *Bulletin of Mathematical Biology*, *60*, 857–899.

Balding, D., & McElwain, D. L. S. (1985). A mathematical model of tumour-induced capillary growth. *Journal of Theoretical Biology*, *114*(1), 53–73.

Bray, D. (1992). *Cell movements*. New York: Garland Publishing.

Byrne, H. M., & Chaplain, M. A. J. (1995). Mathematical models for tumour angiogenesis: numerical simulations and nonlinear wave solutions. *Bulletin of Mathematical Biology*, *57*(3), 461–486.

Byrne, H. M., Chaplain, M. A. J., Hopkinson, I., & Evans, D. (2000). Mathematical modelling of angiogenesis in wound healing: comparison of theory and experiment. *Journal of Theoretical Medicine*, *2*, 175–197.

Chaplain, M. A. J. (1995). The mathematical modelling of tumour angiogenesis and invasion. *Acta Biotheoretica*, *43*, 387–402.

Chaplain, M. A. J., McDougall, S. R., & Anderson, A. R. A. (2006). Mathematical modelling of tumor-induced angiogenesis. *Annual Review of Biomedical Engineering*, *8*, 233–257.

Dorrell, M. I., Aguilar, E., & Friedlander, M. (2002). Retinal vascular development is mediated by endothelial filopodia, a preexisting astrocytic template and specific R-cadherin adhesion. *Investigative Ophthalmology & Visual Science*, *43*(11), 3500–3510.

Dyson, M., Young, S. R., Lynch, J. A., & Lang, S. (1992). Comparison of the effects of moist and dry conditions on dermal repair. *Journal of Investigative Dermatology*, *6*, 729–733.

Flegg, J. A., McElwain, D. L. S., Byrne, H. M., & Turner, I. W. (2009). A three species model to simulate application of hyperbaric oxygen therapy to chronic wounds. *PLoS Computational Biology*, *5*(7), e1000451.

Folkman, J. (1995). Angiogenesis in cancer, vascular, rheumatoid and other disease. *Naturalna Medycyna*, *1*(1), 27–31.

Fruttiger, M., Calver, A. R., Krüger, W. H., Mudhar, H. S., Michalovich, D., Takakura, N., Nishikawa, S., & Richardson, W. D. (1996). PDGF mediates a neuron-astrocyte interaction in the developing retina. *Neuron*, *17*(6), 1117–1131.

Gaffney, E. A., Pugh, K., Maini, P. K., & Arnold, F. (2002). Investigating a simple model of cutaneous wound healing angiogenesis. *Journal of Theoretical Biology*, *45*, 337–374.

Gerhardt, H., Golding, M., Fruttiger, M., Ruhrberg, C., Lundkvist, A., Abramsson, A., Jeltsch, M., Mitchell, C., Alitalo, K., Shima, D., & Betsholtz, C. (2003). VEGF guides angiogenic sprouting utilizing endothelial tip cell filopodia. *The Journal of Cell Biology*, *161*(6), 1163–1177.

Levine, H. A., Pamuk, S., Sleeman, B. D., & Nielsen-Hamilton, M. (2001). Mathematical modeling of the capillary formation and development in tumor angiogenesis: penetration into the stroma. *Bulletin of Mathematical Biology*, *63*(5), 801–863.

Macklin, P., McDougall, S. R., Anderson, A. R. A., Chaplain, M. A. J., Cristini, V., & Lowengrub, J. (2009). Multiscale modelling and nonlinear simulation of vascular tumour growth. *Journal of Mathematical Biology*, *58*, 765–798.

Maggelasis, S. A., & Savakis, A. E. (1996). A mathematical model of growth factor induced cappilary growth in the Retina. *Mathematical and Computer Modelling*, *24*(7), 33–41.

Matzavinos, A., Kao, C. Y., Green, J. E. F., Sutradhar, A., Miller, M., & Friedman, A. (2009). Modeling oxygen transport in surgical tissue transfer. *Proceedings of the National Academy of Sciences of the United States of America*, *106*, 12091–12096.

McDougall, S. R., Anderson, A. R. A., Chaplain, M. A. J., & Sherratt, J. A. (2002). Mathematical modelling of flow through vascular networks: implications for tumour-induced angiogenesis and chemotherapy strategies. *Bulletin of Mathematical Biology*, *64*, 673–702.

McDougall, S. R., Anderson, A. R. A., & Chaplain, M. A. J. (2006). Mathematical modelling of dynamic adaptive tumour-induced angiogenesis: clinical implications and therapeutic targeting strategies. *Journal of Theoretical Biology*, *241*, 564–589.

Olsen, L., Sherratt, J. A., Maini, P. K., & Arnold, F. (1997). A mathematical model for the capillary endothelial cell-extracellular matrix interactions in wound-healing angiogenesis. *IMA Journal of Mathematics Applied in Medicine and Biology*, *14*, 261–281.

Orme, M. E., & Chaplain, M. A. J. (1997). Two-dimensional models of tumour angiogenesis and anti-angiogenesis strategies. *IMA Journal of Mathematics Applied in Medicine and Biology*, *14*, 189–205.

Owen, M. R., Alarcón, T., Maini, P. K., & Byrne, H. M. (2009). Angiogenesis and vascular remodelling in normal and cancerous tissues. *Journal of Mathematical Biology*, *58*, 689–721.

Pettet, G. J., Byrne, H. M., McElwain, D. L., & Norbury, J. (1996a). A model of wound-healing angiogenesis in soft tissue. *Mathematical Biosciences*, *136*(1), 35–63.

Pettet, G., Chaplain, M. A. J., McElwain, D. L. S., & Byrne, H. M. (1996b). On the role of angiogenesis in wound healing. *Proceedings of the Royal Society of London. Series B, Biological Sciences*, *263*, 1487–1493.

Schugart, R. C., Friedman, A., & Chandan, K. S. (2008). Wound angiogenesis as a function of tissue oxygen tension: a mathematical model. *Proceedings of the National Academy of Sciences of the United States of America*, *105*(7), 2628–2633.

Sherratt, JA, & Murray, J. D. (1992). Epidermal wound healing: the clinical implications of a simple mathematical model. *Cell Transplantation*, *1*, 365–371.

Stéphanou, A., McDougall, S. R., Anderson, A. R. A., & Chaplain, M. A. J. (2005). Mathematical modelling of flow in 2D and 3D vascular networks: applications to anti-angiogenic and chemotherapeutic drug strategies. *Mathematical and Computer Modelling*, *41*, 1137–1156.

Stéphanou, A., McDougall, S. R., Anderson, A. R. A., & Chaplain, M. A. J. (2006). Mathematical modelling of the influence of blood rheological properties upon adaptative tumour-induced angiogenesis. *Mathematical and Computer Modelling*, *44*, 96–123.

Stokes, C. L., Rupnick, M. A., Williams, S. K., & Lauffenburger, D. A. (1990). Chemotaxis of human microvessel endothelial cells in response to acidic fibroblast growth factor. *Labor & Investments*, *63*(5), 657–668.

Stone, J., Itin, A., Alon, T., Pe'er, J., Gnessin, H., Chan-Ling, T., & Keshet, E. (1995). Development of retinal vasculature is mediated by hypoxia-induced vascular endothelial growth factor (VEGF) expression by neuroglia. *The Journal of Neuroscience*, *15*, 4738–4747.

Uemura, A., Kusuhara, S., Wiegand, S. J., Yu, R. T., & Nishikawa, S. (2006). Tlx acts as a proangiogenic switch by regulating extracellular assembly of fibronectin matrices in retinal astrocytes. *The Journal of Clinical Investigation*, *116*(2), 369–377.

West, H., Richardson, W. D., & Fruttiger, M. (2005). Stabilization of the retinal vascular network by reciprocal feedback between blood vessels and astrocytes. *Development*, *132*(8), 1855–1862.

Xue, C., Friedman, A., & Sen, C. K. (2009). A mathematical model of ischemic cutaneous wounds. *Proceedings of the National Academy of Sciences of the United States of America*, *106*(39), 16782–16787.